Extreme Weather Events over Hawaii and Western United States in February 2019 Linked to Persistent Ridging over the North Pacific

Center for Western Weather and Water Extremes

Blocking and Extreme Weather in a Changing Climate Workshop
Poster Session #1
Monday 18 March 2024

Tyler Leicht* and Lance Bosart
University at Albany, SUNY
Department of Atmospheric and Environmental Sciences
***Email**: tleicht@albany.edu

UNIVERSITY AT ALBANY
State University of New York

1. Motivation

- Multiple extreme weather events (EWEs) occurred during February 2019
  - Kona low development (9–11 February)
  - Seattle snowfall (10–11 February)
  - Southern California atmospheric river (13–15 February)
  - Arizona and Oregon snowfall (21–25 February)
  - California and Oregon heavy rainfall (26–28 February)

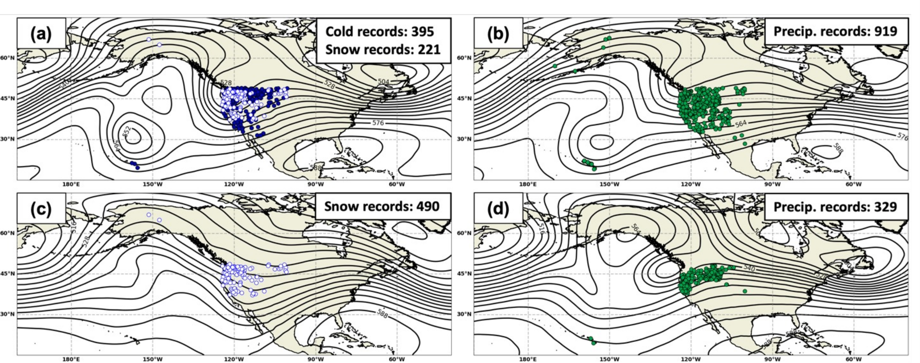

Fig. 1. Time-mean 500-hPa geopotential height (contour, dam) and observed daily weather records for (a) 9–11 February 2019, (b) 9–14 February 2019, (c) 21–25 February 2019, and (d) 26–28 February 2019. Daily records included are low temperature (dark blue), snowfall (white), and precipitation (green).

- Current work aims to analyze the EWEs and a persistent flow regime across the NPAC basin in an extended case study on synoptic and subseasonal-to-seasonal (S2S) timescales

2. Large-Scale Flow Evolution

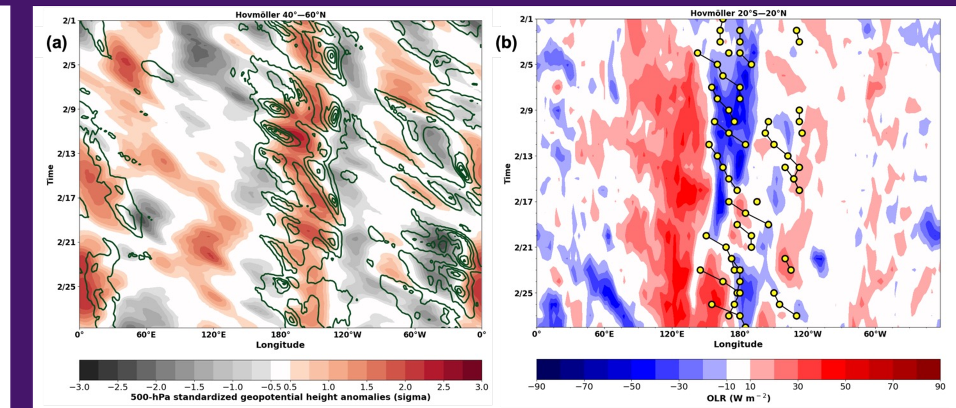

Fig. 2. Hovmöller diagrams of (a) 500-hPa standardized geopotential height anomalies (shaded, sigma) and 700-hPa eddy kinetic energy (contour, $m^2\ s^{-2}$) averaged from 40–60°N and (b) outgoing longwave radiation anomalies (shaded, W m^{-2}) averaged from 20°S–20°N and manual cyclone tracks (yellow dots) for cyclones over the North Pacific basin throughout the month of February 2019.

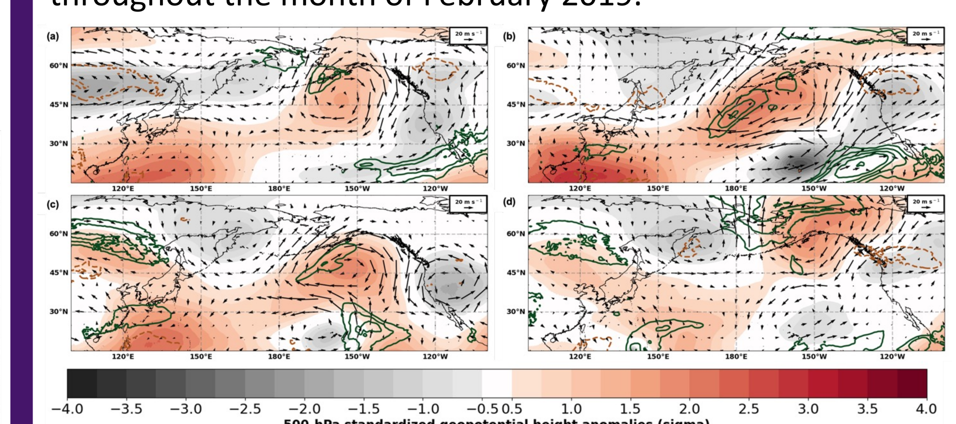

Fig. 3. Mean 500-hPa standardized geopotential height anomalies (shaded, sigma), standardized precipitable water anomalies (contour, sigma), and 250-hPa anomalous wind speed (vector, m s^{-1}) for (a) 1–7 February 2019, (b) 8–14 February 2019, (c) 15–21 February 2019, and (d) 22–28 February 2019.

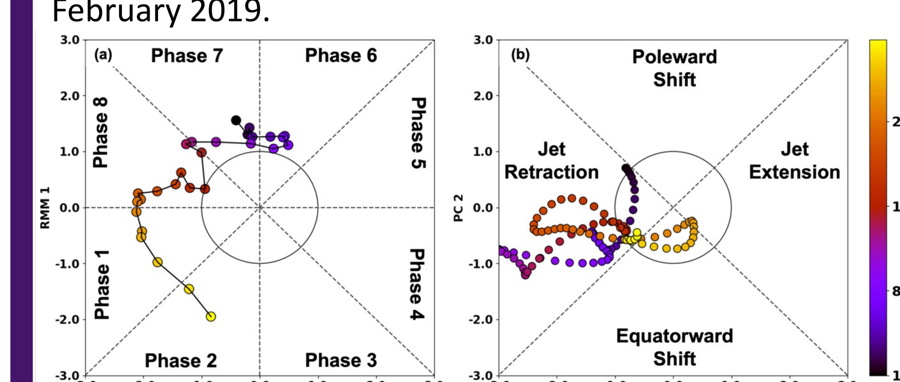

Fig. 4. Phase and amplitude of the (a) Madden–Julian Oscillation and (b) North Pacific jet stream during February 2019.

3. Synoptic Flow Evolution

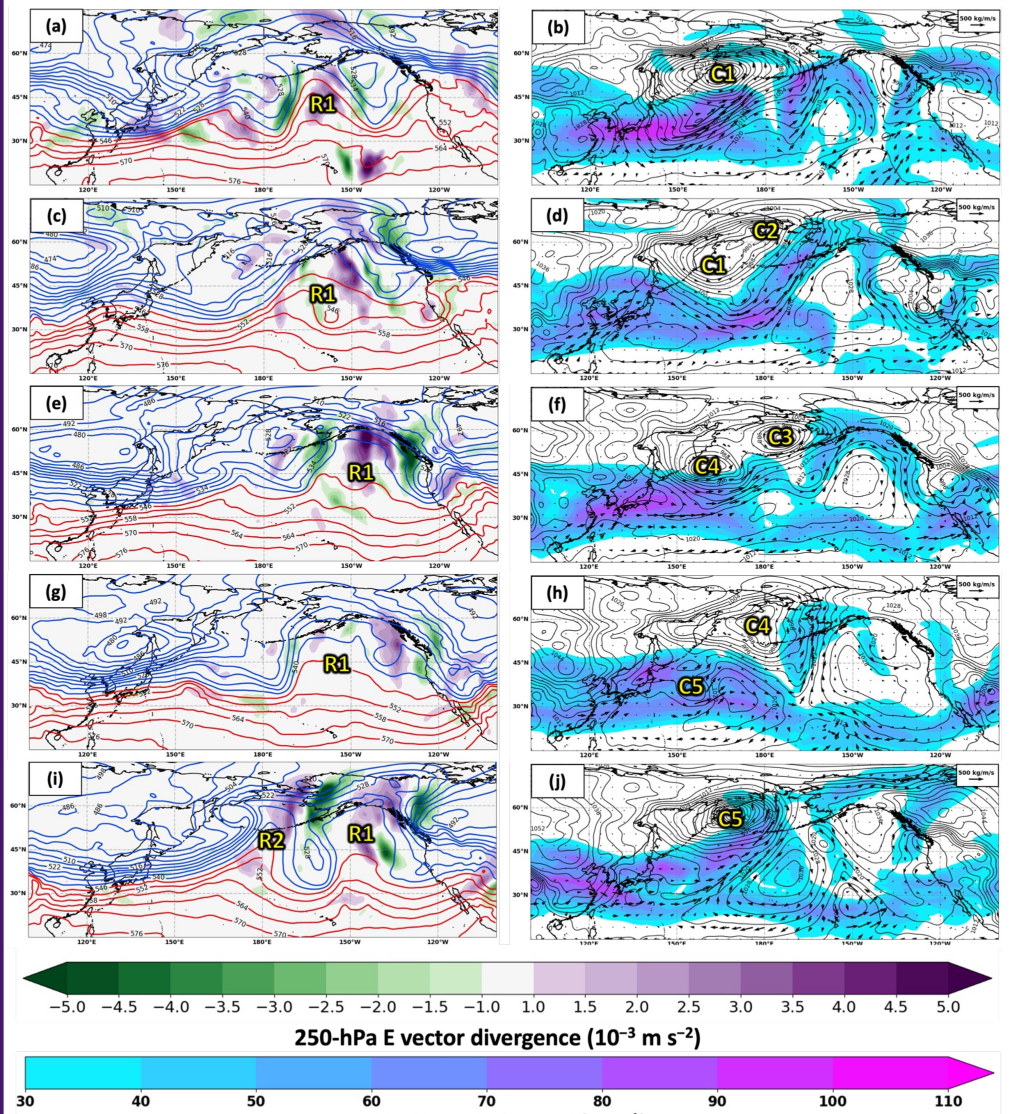

Fig. 5. Large scale flow evolution preceding western US extreme weather events. Left: 1000–500-hPa thickness (contour, dam) and 250-hPa E-vector divergence (shaded, 10^{-3} m s^{-2}) for 0000 UTC on (a) 1 February 2019, (c) 3 February 2019, (e) 5 February 2019, (g) 7 February 2019, and (i) 9 February 2019. Right: Mean sea level pressure (contour, hPa), 250-hPa wind speed (shaded, m s^{-1}), and integrated vapor transport (IVT, vectors, kg $m^{-1}\ s^{-1}$) for 0000 UTC on (b) 1 February 2019, (d) 3 February 2019, (f) 5 February 2019, (h) 7 February 2019, and (j) 9 February 2019. Select cyclones and ridges within the NPAC are labeled for ease of reference.

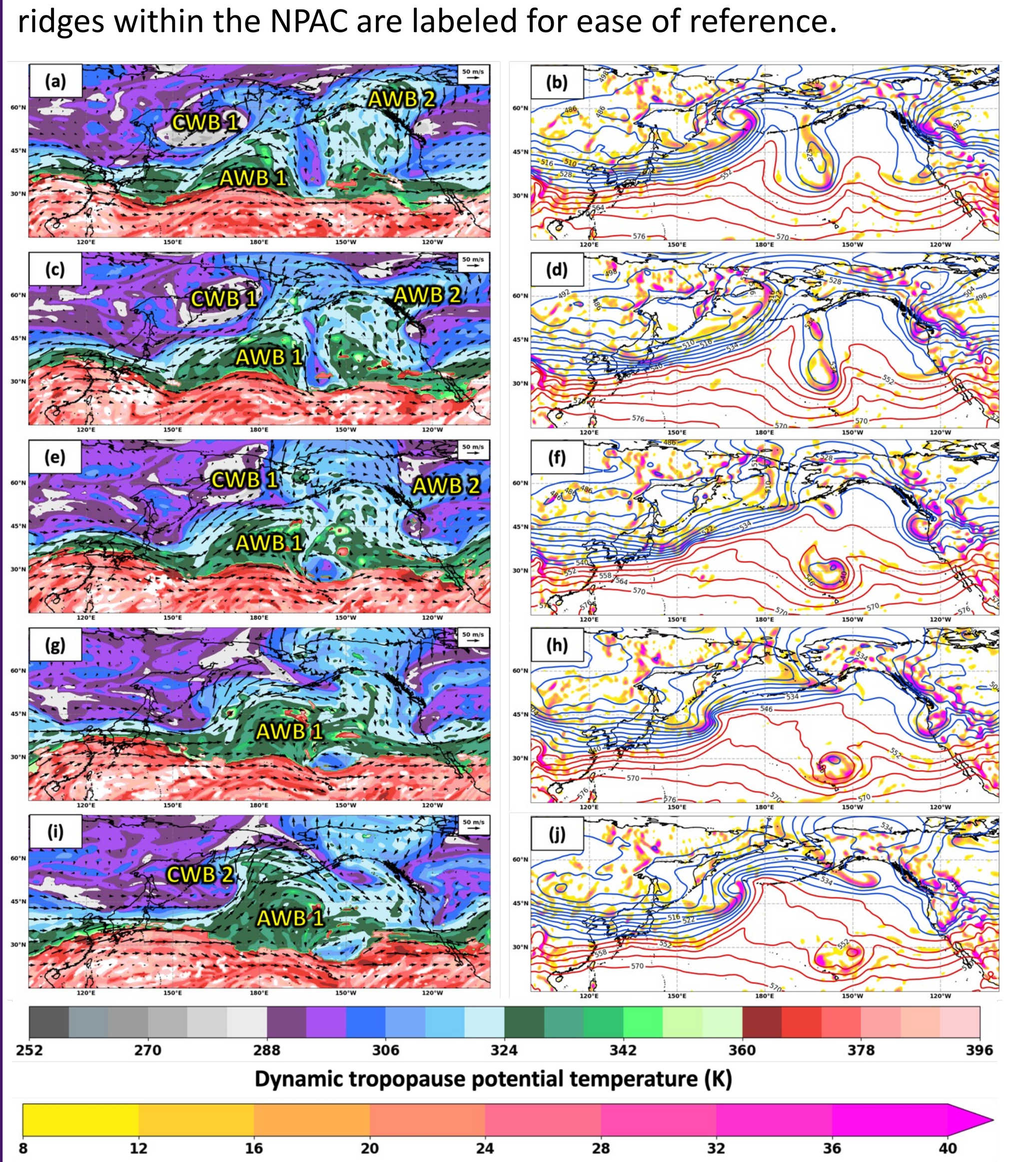

Fig. 6. Kona low development across the central North Pacific basin. Left: Dynamic tropopause potential temperature (shaded, K) and wind speed (vector, m s^{-1}) for (a) 0000 UTC 9 February 2019, (c) 1200 UTC 9 February 2019, (e) 0000 UTC 10 February 2019, (g) 1200 UTC 10 February 2019, and (i) 0000 UTC 11 February 2019. Right: 1000–500-hPa thickness (red/blue contours, dam) and thermal vorticity (shaded, $10^{-5}\ s^{-1}$) for (b) 0000 UTC 9 February 2019, (d) 1200 UTC 9 February 2019, (f) 0000 UTC 10 February 2019, (h) 1200 UTC 10 February 2019, and (j) 0000 UTC 11 February 2019. Select instances of Rossby wave breaking are labeled by their type for ease of reference.

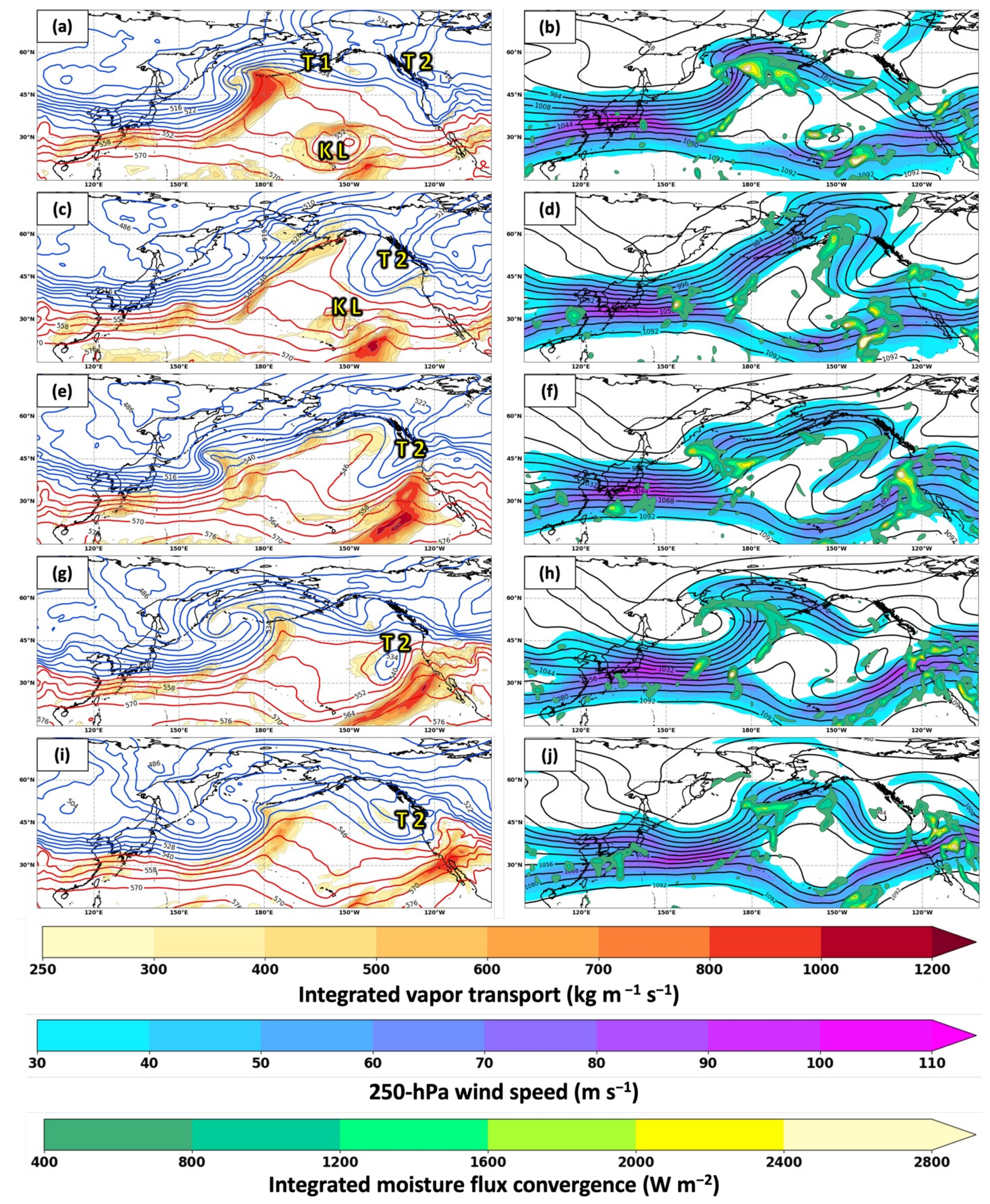

Fig. 7. Left: 1000–500-hPa thickness (red/blue contours, dam) and integrated vapor transport (IVT, shaded, kg $m^{-1}\ s^{-1}$) for (a) 0000 UTC 11 February 2019, (c) 0000 UTC 12 February 2019, (e) 0000 UTC 13 February 2019, (g) 0000 UTC 14 February 2019, and (i) 0000 UTC 15 February 2019. Right: 250-hPa geopotential height (contour, dam), 250-hPa wind speed (shaded, m s^{-1}), and integrated moisture flux convergence (shaded, W m^{-2}) for (b) 0000 UTC 11 February 2019, (d) 0000 UTC 12 February 2019, (f) 0000 UTC 13 February 2019, (h) 0000 UTC 14 February 2019, and (j) 0000 UTC 15 February 2019. Select troughs and upper-level lows are labeled for ease of reference.

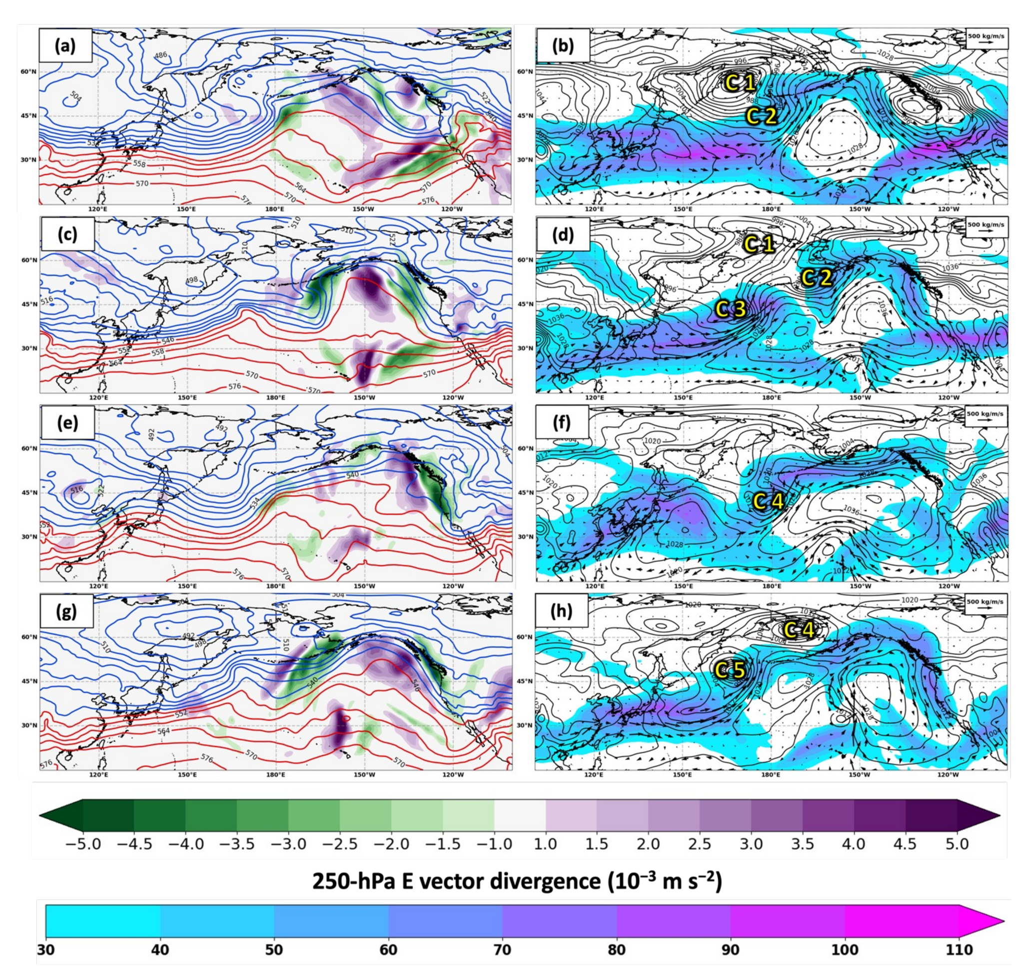

Fig. 8. Large scale flow evolution preceding western US extreme weather events. Left: 1000–500-hPa thickness (contour, dam) and 250-hPa E-vector divergence (shaded, 10^{-3} m s^{-2}) for (a) 0000 UTC 15 February 2019, (c) 0000 UTC 17 February 2019, (e) 0000 UTC 19 February 2019, and (g) 0000 UTC 21 February 2019. Right: Mean sea level pressure (contour, hPa), 250-hPa wind speed (shaded, m s^{-1}), and integrated vapor transport (IVT, vectors, kg $m^{-1}\ s^{-1}$) for (b) 0000 UTC 15 February 2019, (d) 0000 UTC 17 February 2019, (f) 0000 UTC 19 February 2019, and (h) 0000 UTC 21 February 2019.

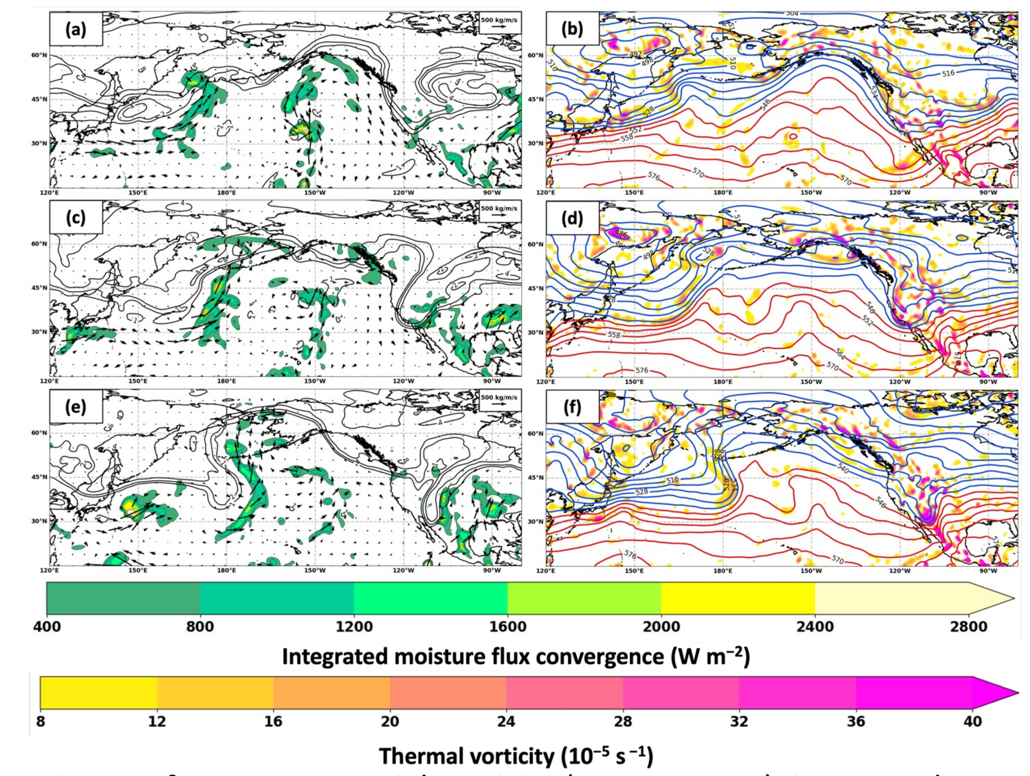

Fig. 9. Left: 310-K potential vorticity (contour, PVU), integrated vapor transport (IVT, vectors, kg $m^{-1}\ s^{-1}$), and integrated moisture flux convergence (shaded, W m^{-2}) for (a) 0000 UTC 21 February 2019, (c) 0000 UTC 22 February 2019, and (e) 0000 UTC 23 February 2019. Right: 1000–500-hPa thickness (red/blue contours, dam) and thermal vorticity (shaded, $10^{-5}\ s^{-1}$) for (b) 0000 UTC 21 February 2019, (d) 0000 UTC 22 February 2019, and (f) 0000 UTC 23 February 2019.

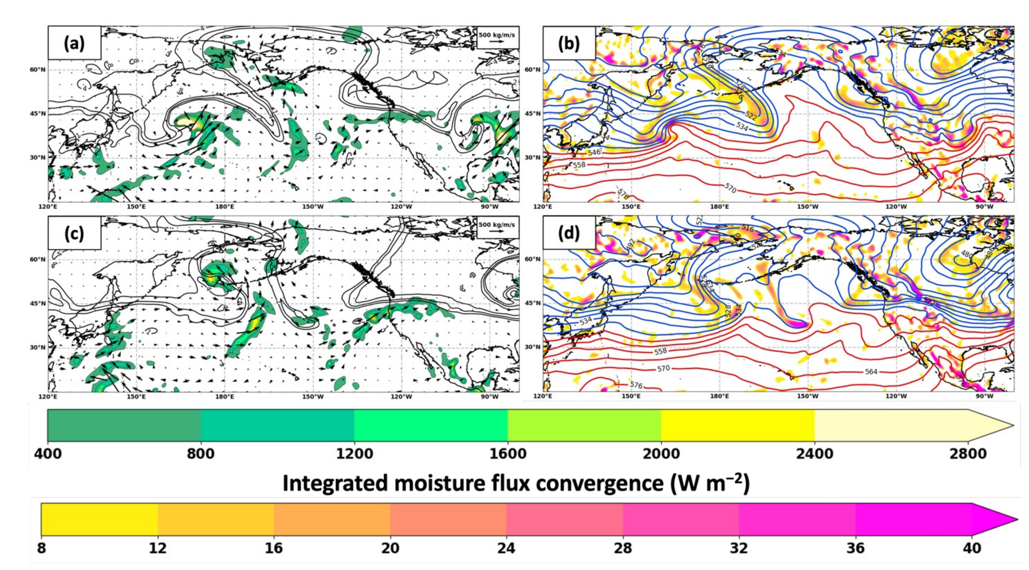

Fig. 10. As in Fig. 9 but for (a), (b) 0000 UTC 24 February 2019 and (c), (d) 0000 UTC 25 February.

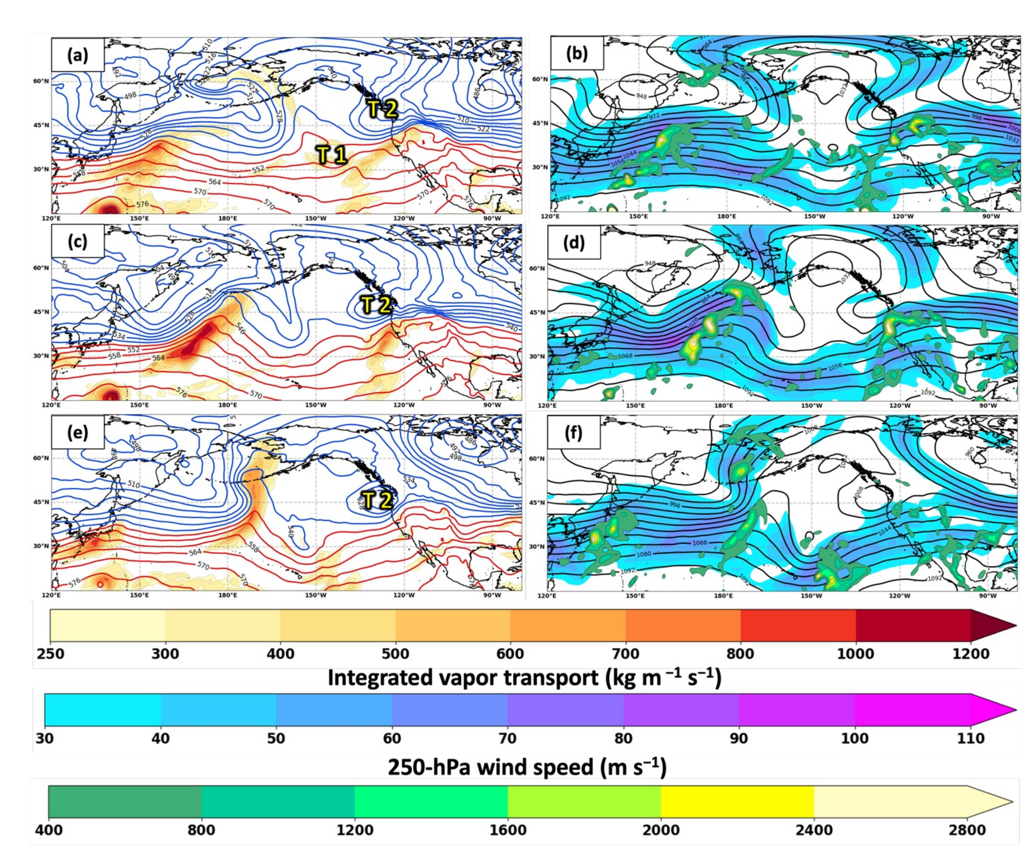

Fig. 11. Left: 1000–500-hPa thickness (red/blue contours, dam) and integrated vapor transport (IVT, shaded, kg $m^{-1}\ s^{-1}$) for (a) 0000 UTC 26 February 2019, (c) 0000 UTC 27 February 2019, and (e) 0000 UTC 28 February 2019. Right: 250-hPa geopotential height (contour, dam), 250-hPa wind speed (shaded, m s^{-1}), and integrated moisture flux convergence (shaded, W m^{-2}) for (b) 0000 UTC 26 February 2019, (d) 0000 UTC 27 February 2019, and (f) 0000 UTC 28 February 2019. Select troughs and upper-level lows are labeled for ease of reference.

4. Summary Schematic

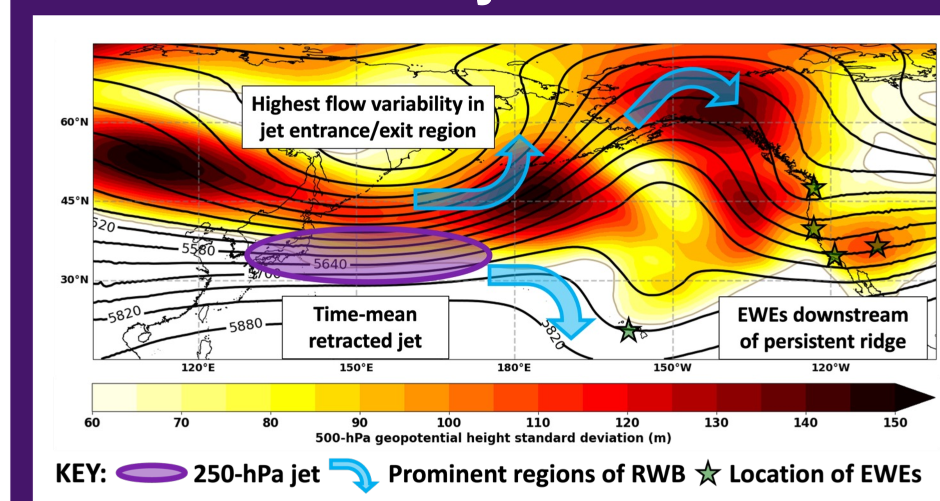

Fig. 12. Schematic depiction of key dynamical drivers for the observed EWEs in February 2019. Monthly averaged 500-hPa geopotential height (contour, m) and the standard deviation of the 500-hPa geopotential height (shaded, m) for February 2019, with annotations for the mean position of the jet, locations of RWB, and the observed EWEs included in this analysis.

5. Discussion

- A new style of case study examining synoptic interactions on the S2S timescales
- Persistent OLR anomalies, the MJO in phases 6 and 7, and a predominantly retracted NPAC jet stream all created conducive background conditions for the EWEs to occur
- Complex interactions between upstream cyclones in the WPAC, a persistent ridge in the CPAC, and Rossby wave breaking across the NPAC contributed to the formation of the EWEs mentioned above
- The synoptic flow evolution highlights the complex mechanisms required to maintain a long-duration weather regime when examined on synoptic timescales
- Ongoing work being performed to understand the composite formation and evolution of other persistent flow regimes

Acknowledgements

Supported by grants from the Center for Western Weather and Water Extremes, Scripps Institute for Oceanography, UC-San Diego #S9002506 and #703813